HHS Public Access

Author manuscript

Angew Chem Int Ed Engl. Author manuscript; available in PMC 2019 October 22.

Published in final edited form as:

Angew Chem Int Ed Engl. 2018 October 22; 57(43): 14101–14105. doi:10.1002/anie.201808074.

Hybrid of Near-Infrared Semiconducting Polymer Brush and pH/GSH-responsive Polyoxometalate Cluster for Enhanced Tumor-Specific Phototheranostics

Zhen Yang[1,2,3], **Wenpei Fan**[3], **Wei Tang**[3], **Zheyu Shen**[3], **Yunlu Dai**[3], **Jibin Song**[3], **Zhantong Wang**[3], **Yuan Liu**[3], **Lisen Lin**[3], **Lingling Shan**[3], **Yijing Liu**[3], **Orit Jacobson**[3], **Pengfei Rong**[1,2], **Wei Wang**[1,2], and **Xiaoyuan Chen**[3]

[1]Cell Transplantation and Gene Therapy Institute, The Third Xiangya Hospital, Central South University, Changsha, Hunan, China.

[2]Engineering and Technology Research Center for Xenotransplantation of Human Province, Changsha, Hunan, China.

[3]Laboratory of Molecular Imaging and Nanomedicine (LOMIN), National Institute of Biomedical Imaging and Bioengineering (NIBIB), National Institutes of Health (NIH), Bethesda, MD 20892, USA

Abstract

Tumor-specific phototheranostics is conducive to realizing precise cancer therapy. Herein, we rationally designed a novel tumor microenvironment (TME)-responsive phototheranostic paradigm based on an excellent match-up of semiconducting polymer brush and polyoxometalate cluster (SPB@POM). On the one hand, the acidic TME could drive the self-assembly of SPB@POM into bigger aggregates for enhanced tumor retention and accumulation. On the other hand, the reductive TME could significantly enhance the NIR absorption of SPB@POM for significant improvement of photoacoustic imaging contrast and photothermal therapy efficacy. Therefore, the intelligent acidity/reducibility dual-responsive SPB@POM allows for remarkable phototheranostic enhancement under the unique TME, which serves as a representative paradigm of nanotechnology in the judicious design of organic/inorganic hybrid nanomaterials for precise tumor-specific phototheranostics with minimal side effects.

Precise semiconducting phototheranostics:

The Hybrid of organic semiconducting polymer brush and inorganic Mo-based polyoxometalate cluster (POM) built an intelligent acidity/reducibility dual-responsive hybrid phototheranostic nanoplatform for *in-situ* self-assembly, enhanced tumor accumulation *and* tumor-specific phototheranostics with largely reduced side effects.

*cjr.wangwei@vip.163.com.

+These authors contributed equally to this work

Supporting information for this article is given via a link at the end of the document.

Conflict of interest

The authors declare no conflict of interest.

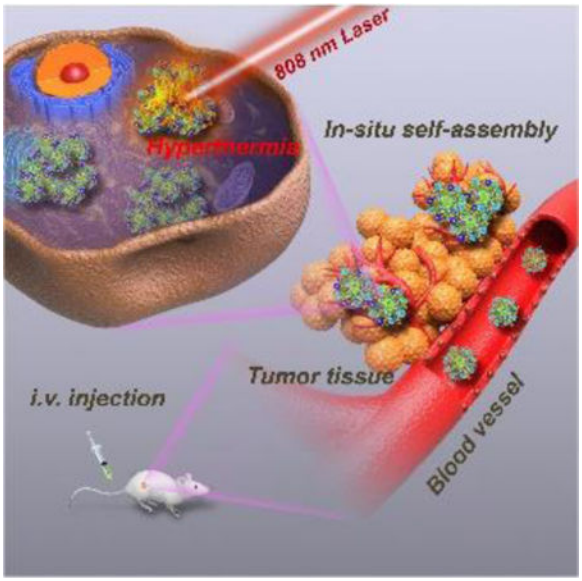

Keywords

semiconducting polymer; tumor microenvironment responsive; photoacoustic imaging; photothermal therapy; phototheranostics

As an emerging noninvasive theranostic protocol for cancer, phototheranostics based on the integration of light-activated diagnosis and therapy, has attracted extensive attention in recent years.[1] Featured with highly polarizable π-systems, near-infrared (NIR)-absorbing organic semiconducting polymers (SPs) have become an outstanding phototheranostic paradigm for photoacoustic (PA) imaging and photothermal therapy (PTT) of carcinoma.[2] Distinct from most inorganic phototheranostic agents (*e.g.,* gold-based nanoagents, carbon-based materials, *etc.*), SPs exhibit high thermal stability and strong phototheranostic performances.[2] However, some inherent issues remain to hinder their practical applications in the clinic. For example, conventional water-soluble SP nanoparticles (SPNs) fabricated by nano-coprecipitation exhibit poor stability under physiological condition.[3] As SPs are usually encapsulated by typical amphiphilic molecules, the formed binary micelles readily undergo dissociation in the presence of proteins and/or other substance during circulation in the blood stream, which inevitably causes a threat to normal tissues.[4] As such, considerable efforts have been devoted to constructing stable SPN through self-assembly of the amphiphilic SPs. During the synthetic process, the backbones of SPs are covalently conjugated with hydrophilic brushes *via* strong covalent bonding force, which can prevent self-dissociation.[5] Another intractable problem is that the SPNs are usually uptaken by tumor-adjacent tissues owing to the relatively low passive targeting efficiency, which is a significant cause of mis-hyperthermia of noncancerous regions during PTT.[6] Although active targeting strategies have proven effective in realizing tumor-targeted delivery of nanoparticles, the high-cost synthesis of targeting ligands/antibodies and complicated procedures of surface modification force us to rethink the simple yet elegant passive targeting strategy based on the EPR effect,[7] which can achieve the win-win of enhanced

tumor accumulation and reduced injection dosage of SPNs, thus minimizing the off-target hyperthermia.

Tumor microenvironment (TME) demonstrates a unique reductive and acidic atmosphere different from normal tissues.[8] As a representative acidity/reducibility-responsive inorganic phototheranostic paradigm, molybdenum (Mo)-based POM clusters with self-adaptive electronic structure exhibit strong NIR absorption through GSH-triggered Mo(VI) to Mo(V) conversion.[9] However, the small-molecule-like POM (≈1 nm) usually suffers from poor EPR effect owing to the rapid removal by mononuclear phagocyte systems.[10] Fortunately, this typical kind of Mo-based POM can form large aggregates in the tumor microenvironment (TME) through protonation-induced hydrogen bonding, which favors its prolonged intratumoral retention. The anchoring of POM onto the surface of SPNs is strongly believed to realize the intratumoral self-assembly of SPNs for enhanced tumor accumulation *via* improved EPR effect. In the meantime, the reductive TME can "reproduce" the strong NIR absorption of POM to amplify the phototheranostic performance of the whole SPN/POM system, which is conducive to achieving pH/GSH dual-responsive precise cancer phototheranostics with largely reduced theranostic dosage. Nevertheless, some challenges remain to be overcome for the judicious design of an outstanding SPN/POM hybrid nanoplatform. First, only the excellent match-up of the absorptions (at around 808 nm) of reduced POM and SP can lead to the cooperative phototheranostic enhancement of the whole system.[11] Second, high-density of thiol groups must be present in the SP brushes (SPB) to chelate sufficient POMs during the formation of SPN@POM nanostructure. Third, a special method should be explored to fabricate such unique SPB with high-density functional brushes.

In this study, a new paradigm of SPB has been first designed and successfully fabricated with the SP backbone (synthesized *via* Stille coupling polymerization[12]) consisting of electron-rich (9-hydroxyl group modified fluorine(F-OH)) and electron-deficient (diketopyrrolopyrrole (DPP)) segments. The brushes were modified with functional groups through atom transfer radical polymerization (ATRP) reaction (Scheme S1).[13] Owing to the metal-thiol coordination chemistry, the widespread thiol groups within SPB could link plenty of POM clusters. Then the hybrid SPB@POM nanoplatform was formed *via* the self-assembly of an amphiphilic complex of POM and SPB during the DMSO dialysis (Scheme 1). The low pH-responsive protonation of POM would drive the *in-situ* self-assembly of SPB@POM in the acidic TME for enhanced intratumoral retention and accumulation. Furthermore, the reductive TME could mostly intensify the NIR absorption of SPB@POM for significantly increased PA imaging contrast and PTT efficiency. Such acidic/reductive TME-responsive SPB@POM are expected to achieve more enhanced tumor accumulation and tumor-specific phototheranostics, thus releasing the renaissance of more precise cancer therapy with minimal adverse effects.

For the fabrication of excellent SPB@POM, the NIR absorption of SPB must match up with that of reductive POM. Thus, the photophysical properties of SP were investigated to optimize the SP backbone by exquisitely tuning the ratio of electron deficient units to electron donators (figure 1a). The band-gaps were forecasted by density functional theory (DFT) calculation based on Gaussian 09 (Figure 1b).[14] Both SP1 and SP2 owed linear

structure with coplanarization of donor and acceptor (D-A) repeating units and delocalization electronic cloud, which demonstrated the strong interaction between D-A. By comparison of the HOMO-LUMO band-gaps of SP1 and SP2, the SP1 had narrower band-gap (ΔEg=1.61 eV). It is such narrow band-gap that gifted the SP a red-shifted absorption peak at 808 nm, which coincided with the absorption of reduced POM at pH 6.5 (Figure 1c). Therefore, the SP1 and POM could be “married” to improve the photoproperties of their hybrid nanoparticles at around 808 nm.

The ATRP macroinitiator was prepared through further hydroxyl modification of SP1 with 2-bromoisobutyryl bromide.[15] The successful syntheses of SPB macroinitiator and SPBs were confirmed by proton nuclear magnetic resonance (^{1}HNMR) spectra and gel permeation chromatography (GPC) (Table S1,Figure S1–9, Supporting Information). The abundant thiol groups in the brush were obtained by amidation of mercaptopropionic acid to the amine groups, and could be used for chelating ^{64}Cu and anchoring POM.

The spherical SPB@POM exhibited high dispersity at pH 7.4 with narrow hydrated size distribution centered at 100 nm (Figure 2b). The elemental mapping showed the homogeneous distribution of POM within the whole structure of SPB@POM (Figure 2c and Figure S10, Supporting Information). The high density of POM in the SPB@POM was expected to feature the whole nanoplatform with acidity-induced aggregation (Figure 2a, Figure S11, Supporting Information).[8] The TEM images (Figure 2e, 2f, 2g), and DLS size changes (Figure 2d) clearly showed the serious aggregation of SPB@POM in acidic solutions with decreasing pH values. Especially, the appearing green precipitates of SPB@POM at pH 3 further validated the acidity-activated aggregation feature of SPB@POM (Figure 3a), which did benefit to its prolonged intratumoral retention for enhanced EPR effect.

Subsequently, the optical properties of SPB and SPB@POM were studied under physiological conditions. The absorbance of SPB@POM was gradually elevated with time in GSH solution (Figure 3b). After 6 h incubation, the absorption of SPB@POM showed almost 2-fold enhancement compared with that of the original SPB@POM. After transferring the reduced SPB@POM to PBS at pH 6.5, the maximal absorption peak at 808 nm exhibited excellent match-up with that of reduced POM (Figure S12, Supporting Information). The color of SPB@POM solutions under different pH values changed from jade green to navy blue after incubation with GSH (Figure 3a). Upon 808 nm laser excitation, the PA contrast of SPB@POM was enhanced 1.8-fold or 2.2-fold after incubation with 10 mM GSH at pH 7.4 or 10 mM GSH at pH 6.5 by comparison with that before incubation (Figure 3c). This phenomenon could be ascribed to the acidity-triggered aggregation of SPB@POM that resulted in an increased local concentration for PA enhancement. After 5 min of laser irradiation, SPB@POM incubated with or without 10 mM GSH showed a rapid temperature increase to 70 ºC or 57 ºC, respectively. Moreover, SPB@POM incubated with 10 mM GSH at pH 6.5 even reached a high temperature of 77 ºC (Figure 3d). To reach 55 ºC, a temperature for effective tumor ablation, the required concentration of SPB was 2.8-fold than that of SPB@POM under TME mimic condition (Figure S13, Supporting Information). All these results showed that the well-designed SPB@POM could be used for pH/GSH dual-responsive PA imaging and PTT therapy.

In cellular experiments, both SPB and SPB@POM exhibited good biocompatibility (Figure S14, Supporting Information). After irradiation with 808 nm laser for 5 min, the SPB@POM (pre-incubated with 10 mM GSH) could kill all of the cancer cells, but SPB can only kill about half of the cancer cells (Figure S15, S16 and S17, Supporting Information). In vitro experiments showed that the SPB@POM produced much higher PTT effect than the SPB.

The enhanced tumor accumulation of SPB@POM *via in-situ* self-assembly was evaluated by PET imaging and PA imaging. PET imaging was first performed to investigate the pharmacokinetics of SPB@POM in U87MG tumor-bearing mice (Figure 4a). The ^{64}Cu-labeled SPB and SPB@POM were intravenously injected into the mice, and the PET images were captured at 1, 4, 24, 48 h post injection. By comparison with SPB, SPB@POM showed increased tumor uptake and reduced liver uptake at each time point. The highest tumor uptake (%ID/g) of the SPB@POM (9.85±1.23) was about 1.8-fold higher than that of SPB (5.60±0.89) at 24 h (Figure 4b). The biodistribution at 48 h time point was measured by a gamma counter further showed that the tumor accumulation of SPB@POM was 2-fold higher than that of SPB (Figure S18, Supporting Information). The PET imaging results confirmed that POM could significantly promote the tumor accumulation of SPB through the enhanced EPR effect based on intratumoral acidity-driven self-assembly of SPB@POM. Besides, PA imaging was also performed to reflect the tumor uptake of the SPB and SPB@POM. The SPB@POM-treated tumor exhibited almost 3-fold amplified PA intensity than SPB-treated tumor at 24 h post injection (Figure S19, Supporting Information). The dramatic PA enhancement could be attributed to both the acidity-driven aggregation of SPB@POM and the GSH-triggered Mo (VI) to Mo (V) conversion within POM. The tumor-specific PA imaging by acidic/reductive TME-responsive SPB@POM could precisely position the tumor to guide the following PTT treatment.

The strongest PA signal of tumor appeared at 24 h post-injection, at which an 808 nm laser with power density of 0.5 W/cm^2 was used to irradiate the tumor for 5 min. As shown by the IR thermal imaging (Figure 4c), the tumors of mice injected with SPB@POM showed rapid temperature rise to 55 ºC. However, the temperatures of tumors in SPB and saline treated mice only reached 45 and 35 ºC, respectively (Figure 4d). After 808 nm laser irradiation, the SPB@POM could completely inhibit tumor growth and even ablate tumor at day 4 (Figure 4e). The survival of mice treated by SPB@POM plus Laser was substantially extended to over 45 days (Figure 4f). No obvious body weight drop was observed, indicating relatively high bio-safety of all these treatments (Figure S20, Supporting Information). The H&E stained images revealed the healthy major organs but extensive tumor cell apoptosis/necrosis by the treatment of SPB@POM plus Laser (Figure S21 and S22, Supporting Information), which further accounted for the highest treatment efficacy.

In summary, we first developed an intelligent pH/GSH dual-responsive hybrid nanoplatform based on the excellent match up of inorganic POM and organic SP for concurrent tumor-specific self-assembly and phototheranostic enhancement. Several unusual methods were applied to synthesize the hybrid SPB@POM. The well-designed SPB@POM was featured with acidic TME-driven self-aggregation and reductive TME-triggered NIR absorption intensification, thus resulting in improved PA imaging contrast and PTT efficacy. The hybrid of SPB and POM not only resolved the rapid metabolism of ultra-small POM in blood, but

also greatly reduced the dosage of SP, thus achieving an unprecedented phototheranostic efficacy. The unique acidity/reducibility dual-responsiveness of SPB@POM is also expected to illustrate significant guidance on the future design of “magic” tumor-specific phototheranostic nanoplatfotms for precise cancer therapy.

Supplementary Material

Refer to Web version on PubMed Central for supplementary material.

Acknowledgements

This work was financially supported by the Youth Innovation Promotion Association of the Chinese Academy of Sciences (2016269), the Intramural Research Program (IRP) of the NIBIB, NIH, and the National Natural Science Foundation of China (Grant Nos. 81771827, 81471715, 51602203, 51761145021). We are also grateful to Xiangchun Li from Nanjing University of Posts and Telecommunications for density functional theory (DFT) calculations by Gaussian 09.

References

[1]. a) Song J, Yang X, Jacobson O, Huang P, Sun X, Lin L, Yan X, Niu G, Ma Q, Chen X, Adv. Mater. 2015, 27, 4910–4917; [PubMed: 26198622] b) Huang P, Rong P, Jin A, Yan X, Zhang MG, Lin J, Hu H, Wang Z, Yue X, Li W, Adv. Mater. 2014, 26, 6401–6408; [PubMed: 25123089] c) Huang P, Rong P, Lin J, Li W, Yan X, Zhang MG, Nie L, Niu G, Lu J, Wang W, J. Am. Chem. Soc. 2014, 136, 8307–8313; [PubMed: 24842342] d) Cheng L, Wang C, Feng L, Yang K, Liu Z, Chem. Rev. 2014, 114, 10869–10939. [PubMed: 25260098]

[2]. a) Guo B, Sheng Z, Hu D, Li A, Xu S, Manghnani PN, Liu C, Guo L, Zheng H, Liu B, ACS Nano 2017, 11, 10124–10134; [PubMed: 28892609] b) Jiang Y, Li J, Zhen X, Xie C, Pu K, Adv. Mater. 2018, 30, 1705980;c) Lyu Y, Xie C, Chechetka SA, Miyako E, Pu K, J. Am. Chem. Soc. 2016, 138, 9049–9052; [PubMed: 27404507] d) Pu K, Shuhendler AJ, Jokerst JV, Mei J, Gambhir SS, Bao Z, Rao J, Nat. Nanotechnol. 2014, 9, 233–239. [PubMed: 24463363]

[2]. a) Zhen X, Xie C, Pu K, Angew. Chem. Int. Ed. 2018, 130, 4002–4006;b) Zhang J, Yang C, Zhang R, Chen R, Zhang Z, Zhang W, Peng SH, Chen X, Liu G, Hsu CS, Adv. Funct. Mater. 2017, 27, 1605094;c) Li D, Zhang G, Xu W, Wang J, Wang Y, Qiu L, Ding J, Yang X, Theranostics 2017, 7, 4029. [PubMed: 29109796]

[3]. a) Dong T, Wen K, Chen J, Xie J, Fan W, Ma H, Yang L, Wu X, Xu F, Peng A, Adv. Funct. Mater. 2018, 28, 1800135;b) Li J, Rao, Pu K, Biomaterials 2018, 155, 217–235. [PubMed: 29190479]

[4]. Lyu Y, Zeng J, Jiang Y, Zhen X, Wang T, Qiu S, Lou X, Gao M, Pu K, ACS Nano 2018, 12, 1801–1810. [PubMed: 29385336]

[5]. a) Zhang S, Guo W, Wei J, Li C, Liang X-J, Yin M, ACS Nano 2017, 11, 3797–3805; [PubMed: 28301720] b) Xie C, Zhen X, Lei Q, Ni R, Pu K, Adv. Funct. Mater. 2017, 27, 1605397;c) Yang Z, Tian R, Wu J, Fan Q, Yung BC, Niu G, Jacobson O, Wang Z, Liu G, Yu G, ACS Nano 2017, 11, 4247–4255; [PubMed: 28345873] d) Xie C, Zhen X, Miao Q, Lyu Y, Pu K, Adv. Mater. 2018, 30, 1801331.

[6]. Li J, Xie C, Huang J, Jiang Y, Miao Q, Pu K, Angew. Chem. Int. Ed. 2018, 57, 3995–3998.

[7]. Xie C, Zhen X, Lyu Y, Pu K, Adv. Mater. 2017, 29, 1703693.

[8]. a) Zhang C, Ni D, Liu Y, Yao H, Bu W, Shi J, Nat. Nanotech. 2017, 12, 378;b) Estrella V, Chen T, Lloyd M, Wojtkowiak J, Cornnell HH, Ibrahim-Hashim A, Bailey K, Balagurunathan Y, Rothberg JM, Sloane BF, Johnson J, Gatenby RA, Gillies RJ, Cancer Res. 2013, 73, 1–12.; Sun C, Liu Y. Du J, Cao Z, Xu C, Wang J, Angew. Chem. Int. Ed. 2016, 128, 1022–1026. Kuppusamy P, Li H, Ilangovan G, Cardounel AJ, Zweier JL, Yamada K, Krishna MC, Mitchell JB, Cancer Res. 2002, 62, 307–312.

[9]. Zhang C, Bu W, Ni D, Zuo C, Cheng C, Li Q, Zhang L, Wang Z, Shi J, J . Am. Chem. Soc. 2016, 138, 8156–8164. [PubMed: 27264421]

[10]. Ni D, Jiang D, Im H-J, Valdovinos HF, Yu B, Goel S, Barnhart TE, Huang P, Cai W, Biomaterials 2018, 171, 144–152. [PubMed: 29689411]

[11]. Yang Z, Song J, Dai Y, Chen J, Wang F, Lin L, Liu Y, Zhang F, Yu G, Zhou Z, Theranostics 2017, 7, 2177. [PubMed: 28740543]

[12]. Hendriks KH, Heintges GH, Gevaerts VS, Wienk MM, Janssen RA, Angew. Chem. Int. Ed. 2013, 125, 8499–8502.

[13]. Zhang Z, Fan Q, Sun P, Liu L, Lu X, Li B, Quan Y, Huang W, Macromol. Rapid Comm. 2010, 31, 2160–2165.

[14]. Xin H, Ge C, Jiao X, Yang X, Rundel K, McNeill CR, Gao X, Angew. Chem. Int. Ed. 2018, 130, 1336–1340.

[15]. Lu X, Jiang R, Yang M, Fan Q, Hu W, Zhang L, Yang Z, Deng W, Shen Q, Huang W, J. Mater. Chem. B 2014, 2, 376–386.

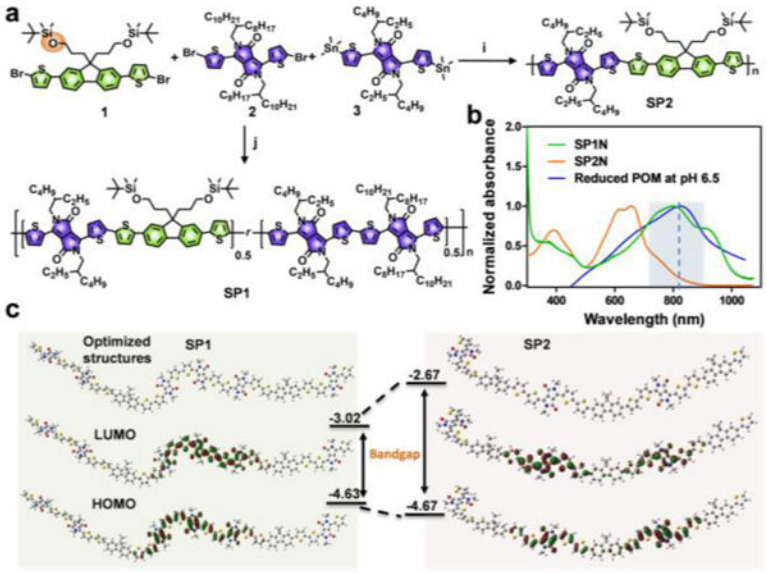

Figure 1.

a) Synthetic route of SP1 and SP2. The ratios of monomer 1, 2 and 3 were 1:1:1 (j) and 1:0:1 (i) for SP1 and SP2, respectively. b) Absorption spectra of SP1N, SP2N and reduced POM at pH 6.5. c) Geometry-optimized structures, and HOMO and LUMO wave functions of SP1 and SP2 (The methyl chains were substituted to amide position of SP1 and SP2 for simplicity.)

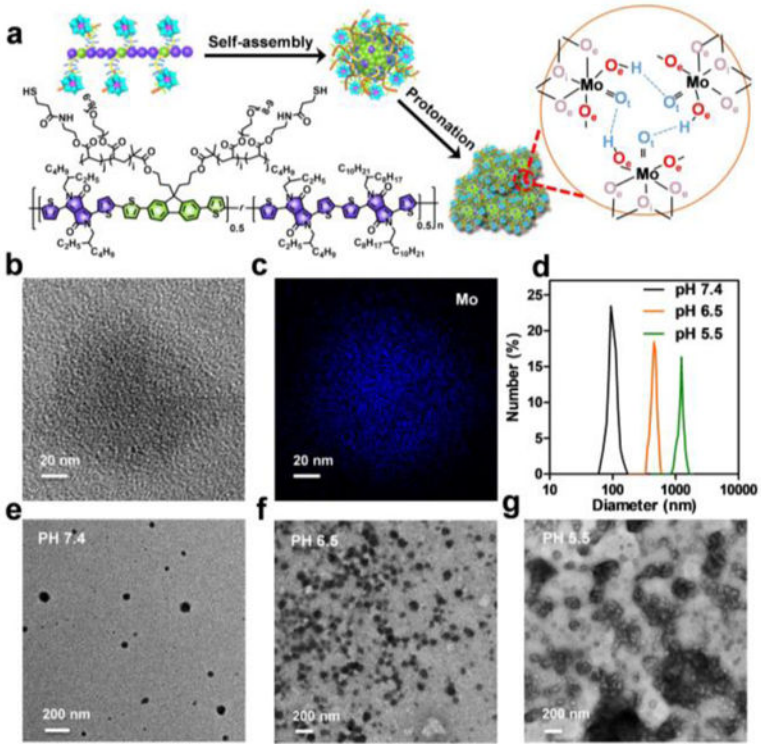

Figure 2.

a) Schematic of the structure of SPB, synthesis of SPB@POM and mechanism of acidity-induced aggregation of SPB@POM. b) High-resolution TME image and c) its corresponding elemental mapping of SPB@POM. d) Dynamic light scattering profiles and e, f, g) TEM images of SPB@POM in solutions with different pH values (pH 7.4, 6.5, and 5.5).

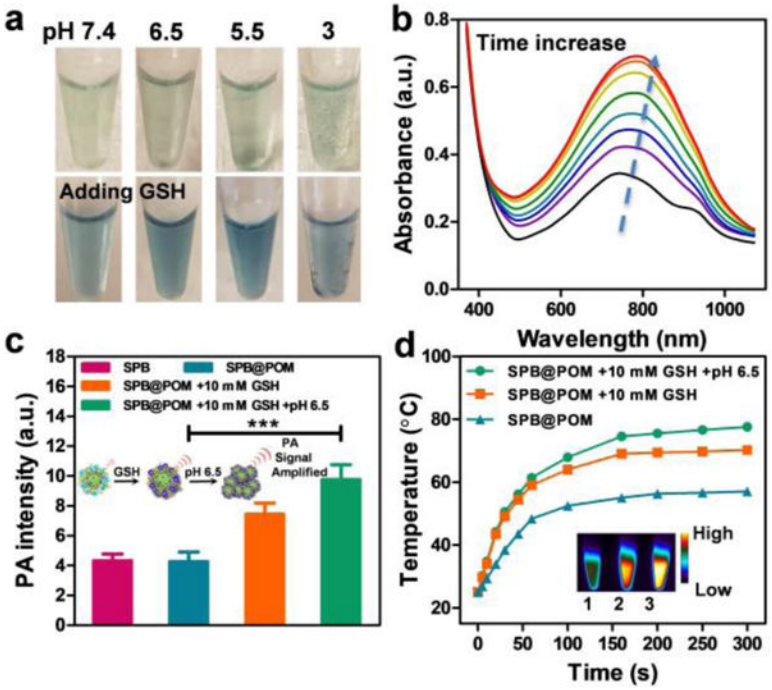

Figure 3.

a) Photographs of SPB@POM solutions with or without addition of GSH under different pH values. b) Absorption spectra of SPB@POM after incubation with 10 mM GSH for increasing time (0, 0.5, 1, 1.5, 2, 4, 6, 12 h). c) PA intensities of SPB, SPB@POM, SPB@POM incubated with 10 mM GSH and SPB@POM with 10 mM GSH at pH 6.5 (insets: schematic of PA amplification by GSH-triggered reduction of POM and low pH-induced protonation of SPB@POM). d) Temperature rise profiles and IR thermal images (insets) of SPB@POM, SPB@POM with 10 mM GSH, and SPB@POM with 10 mM GSH at pH 6.5.***$P<0.001$.

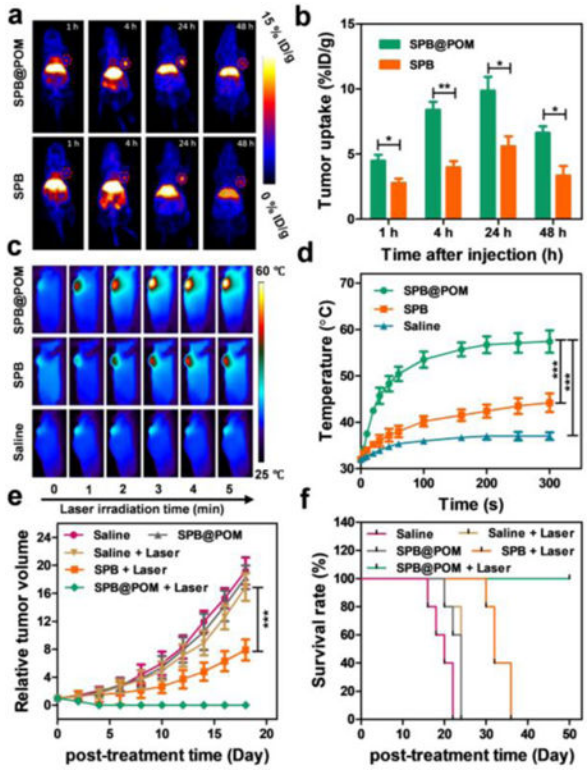

Figure 4.

a) The PET imaging and b) corresponding tumor uptake (%ID/g) of U87MG tumor-bearing mice by *i.v.* injection of SPB and SPB@POM. c) IR thermal imaging of U87MG tumor-bearing mice during 5 min of 808 nm laser irradiation after *i.v.* injection of SPB, SPB@POM and saline. d) Temperature rise profiles of the tumor as a function of the irradiation time. e) Tumor growth curves and f) survival rates of U87MG tumor-bearing mice subjected to varied treatments. **P*<0.05, ***P*<0.01, ****P*<0.001.

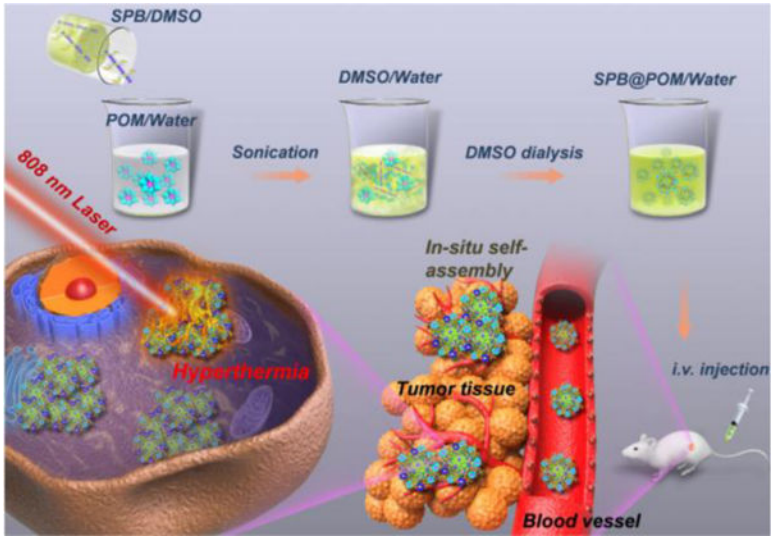

Scheme 1.

Schematic of acidic/reductive TME-responsive SPB@POM for tumor-specific self-assembly and phototheranostic enhancement.